UNSYS digital

Journal of Unmanned System Technology

A Cooperative Navigation Method of Multiple AUVs for Wide Seafloor Survey –First Performance Evaluation in Sea Environments–

Takumi Matsuda†, Toshihiro Maki†, Yoshiki Sato†, Takashi Sakamaki†, Tamaki Ura‡

†Institute of Industrial Science, the University of Tokyo, 4-6-1 Komaba, Meguro-ku, Tokyo, 153-8505 JAPAN

‡Kyushu Institute of Technology, 2-4 Hibikino, Wakamatsu-ku, Kitakyushu-shi, Fukuoka, 808-0196, JAPAN

Abstract— This paper reports the sea experimental results and the performance evaluation of a cooperative navigation method of multiple autonomous underwater vehicles (AUVs). AUVs are divided into two groups: moving and landmark. Moving AUVs estimate their states (horizontal positions and heading angle) from their ground velocity, horizontal angular velocity, and acoustical positioning relative to a landmark AUV remaining stationary on the seafloor. A stochastic approach called a particle filter is adopted for state estimation. Each AUV can navigate with small drift over a wide area by alternating the landmark role. When AUVs exchange their landmark roles, they share their estimated states by compressing states with small communication traffic. The method is implemented in two hovering type AUVs (AUV Tri-Dog 1 and AUV Tri-TON 1). The method was evaluated in sea environments in November 2013. The AUVs succeeded in a cooperative navigation, alternately becoming the landmark. It was verified that the implemented method had the ability to perform the wide seafloor survey only by AUVs through sea experiments and post-processing simulation using the experimental results.

Keywords— localization, multiple AUVs, particle filter

DOI: 10.21535/just.v6i2.1035

I. INTRODUCTION

THIS paper reports the sea experimental results and the performance evaluation of a cooperative navigation method of multiple autonomous underwater vehicles (AUVs). In our previous paper, the method was proposed to conduct wide area surveys near the seafloor only by AUVs [1]. The method was implemented in two hovering type AUVs, and the first experiments in sea environments were conducted using them. In the proposed method, one AUV remains stationary on the seafloor and acts as the landmark for a moving AUV that observe the seafloor. By alternating the landmark role, all AUVs cover a wide area. This study focuses on the seafloor survey using hovering type AUVs.

The key elements of localization and mapping of AUVs were investigated [2], [3]. Several groups proposed control algorithms and navigational guides for single AUVs. Among control algorithms, adaptive pitch control [4], a self-organizing neural-net-controller system [5] were proposed. Among the navigational guides, passive acoustical landmarks [6], GPS buoys [7], and terrain features [8] were previously proposed. These guides enable small-drift observation of well-located targets near positioning references. However, they offer limited observational coverage because their positioning accuracy degrades as the AUV departs from the positioning references. In addition, this limited coverage area limits the number and type of observable targets. AUVs often fail to reach even precisely located targets because they are misled by underwater currents, positioning errors, and other factors. To overcome these problems, we have previously proposed a positioning method for multiple AUVs, in which a moving AUV estimates the state based on a stationary landmark AUV on the seafloor [1]. The central concept is to alternate the moving and landmark roles among the AUVs. This approach was first proposed in Kurazume and Hirose's seminal work [9], where it was referred to as a cooperative positioning system (CPS). The CPS method realizes wide area navigation with small drift by alternating the landmark role among vehicles. However, although CPS has been adopted in land vehicles [10], [11], its application to multiple AUV navigation has not been reported. To realize multiple AUV navigation by CPS, we combined the CPS technique with a stochastic approach (particle filter) [1], [12]. To our knowledge, this is the first application of CPS to multiple AUV navigation.

The navigation of multiple vehicles in land and aerial environments has been extensively investigated, and many navigational methods have been proposed and demonstrated using actual vehicles [10], [11], [13]–[16]. In marine environments, there are fewer researches than in land or aerial environments. In one report, the research group of Woods Hole Oceanographic Institute (WHOI) in USA have conducted the investigation of the Arctic Ocean using two actual AUVs called "JAGUAR" and "PUMA" [17]. In another approach, two moving AUVs realize cooperative positioning from range-only measurements [18]. A navigational method for autonomous surface vehicles has also been proposed [19]. Another group developed an efficient underwater coverage method for multiple AUVs exposed to sea current disturbances [20]. A distributed, context-aware self-organization/reorganization

Corresponding author: Takumi Matsuda
(e-mail: {matsuda,maki,ys-sato,sakamaki}@iis.u-tokyo.ac.jp)

This paper was submitted on March 31, 2014; revised on April 3, 2015; and accepted on May 20, 2015.

scheme for advanced multi-AUV systems was developed [21]. Sea trials using a fleet of autonomous underwater gliders in Monterey Bay were reported [22]. Since cooperative surveys are restricted by the very low bandwidths of the acoustic channel, multiple AUV navigation with small data communication have achieved successful location sharing by the extended Kalman filter method for state estimation, in which the states of the AUVs are simply expressed by matrices [18], [19], [23].

The original contribution of this study is that only AUVs perform the seafloor survey without any surface aid by alternating the landmark role after being deployed. All the AUVs can perform stable localization due to one static landmark AUV. Thus, the method is expected to be a new technology of the seafloor survey requiring accurate positioning, which has been impossible for existing studies. It will become possible for environmental information of wide seafloor, such as seafloor photomosaic, chemical concentration map, and geographical feature map to be obtained by only AUVs.

The navigation method is explained in Section II. Section III explains the implementation of the method in actual AUVs. Section IV presents and discusses the experimental results. This section also evaluates the performance of the method by post-processing simulation of the experimental results. Conclusions and ideas for future work are presented in Section V. This study extends the work of our previous study [24], in which state estimation was refined by particle reconstruction to prevent a moving AUV from incorrectly converging the states.

II. METHOD

A. Navigation

AUVs alternate between the "moving role (MR)" and "landmark role (LR)." A moving AUV estimates the states of both moving and landmark AUVs from navigation sensors and its position relative to a landmark AUV. A mutual acoustical positioning is adopted [25], and the stationary landmark AUV provides a reference that guides the moving AUV. By alternating the LR, all AUVs cover a wide area while maintaining low positioning error.

Figure 1 illustrates the proposed method with two AUVs, labelled A and B. In this figure, AUV A and AUV B adopt the MR and LR, respectively. The procedure is implemented as follows.

1) A observes the seafloor with respect to B, while B remains stationary on the seafloor.
2) Having completed its observation referenced to B, A lands on the seafloor. A transmits compressed information regarding the estimated states to B.
3) B begins observing the seafloor based on the information received from A.

Two AUV case is shown here. To extend the method to more AUV navigation, two AUVs alternate between the moving role and the landmark role (called as "main AUVs"), and other AUVs constantly move based on the landmark AUV (called as "sub AUVs"). All the AUVs can expand the observational coverage since the main AUVs alternate between the moving and landmark roles. Details were explained in our previous paper [26]. Here, we focus on two AUV case (called "main AUVs").

B. AUV's States

An AUV's state is evaluated from six parameters: three-dimensional position (x, y, z), and rotation (roll, pitch, and yaw). The depth z is precisely measured by a pressure sensor. The roll and pitch angles are also measured by an attitude sensor without drift. The horizontal position (x,y) and the heading angle (yaw) (ψ) are not measured and must be estimated.

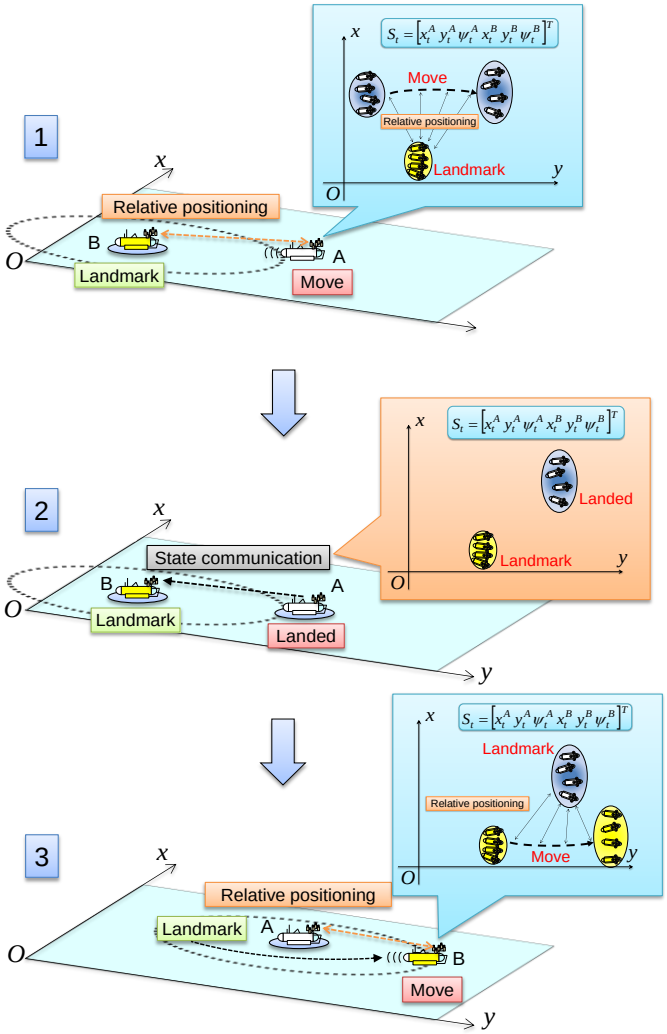

Figure 1 Procedure of the proposed method.

C. State Estimation

We now face the challenge of suppressing the estimation errors. To this end, a stochastic state estimator (such as a particle filter and an extended Kalman filter: EKF) is introduced [12]. The performance of long distance navigation

by multiple AUV navigation using the particle filter and the EKF were compared through the simulation in [27]. It was verified that the particle filter performed robust state estimation against sensor noises compared to the EKF. Here, the particle filter was selected for state estimation to implement. Since the particle filter expresses the state probability density by a set of particles, it is suitable to express a complicated distribution of the state. Several particle filter-based navigation algorithms for vehicular navigation have been proposed, some of which have been implemented in AUVs [1], [6], [8], [24], [25]. As the number of particles increases, the more complicated distributions can easily be expressed. Since the states of the multiple AUVs can multimodally change in the proposed navigation method, the particle filter is suitable for expressing such complicated states.

In the method, the states of both moving and landmark AUVs can be uncertain. The state at time *t* is a composite of the states of the moving and landmark AUVs. It is represented as $S_t = \{\mathbf{s}_t^i \mid i = 1, \cdots, n\}$, where $\mathbf{s}_t^i = \left[x_t^{\mathrm{M}i}\ y_t^{\mathrm{M}i}\ \psi_t^{\mathrm{M}i}\ x_t^{\mathrm{L}i}\ y_t^{\mathrm{L}i}\ \psi_t^{\mathrm{L}i}\right]^{\mathrm{T}}$ denotes the state of the *i*th particle. The moving AUV estimates the state S_t from its own navigation sensors and the positions relative to the landmark AUV. The particle filter updates state S_t through two phases: prediction and observation. In the prediction phase, the moving AUV estimates state S_t from its navigation sensors. The ground velocity sensor and one-axis heading rate gyro provide the ground velocity $\hat{\mathbf{v}}_t$ and the angular velocity $\hat{\omega}_t$, respectively. In the observation phase, the states are updated from relative acoustical positioning measurements between the moving and landmark AUVs [1], [25]. The positioning measurements are the relative distance $\hat{r}_t$ and the relative directions $\hat{\theta}_t^{\mathrm{ML}}$ and $\hat{\theta}_t^{\mathrm{LM}}$, where $\hat{\theta}_t^{\mathrm{ML}}$ is the direction of the moving AUV relative to the landmark AUV, and $\hat{\theta}_t^{\mathrm{LM}}$ is the reverse direction. Using the particle filter, the AUVs realize stable and robust state estimation against sensor noises and lack of measurement data.

The timeline of the state estimation process is shown in Figure 2. The particles are updated by the abovementioned two phases. The observation phase is bypassed when observation data are unavailable. If the moving AUV transmits a positioning signal at time *t*, it receives a response from the landmark AUV at time $t + \Delta t$. This delay is considered in the position-based particle update. The state estimation is detailed in a previous paper [1], [27].

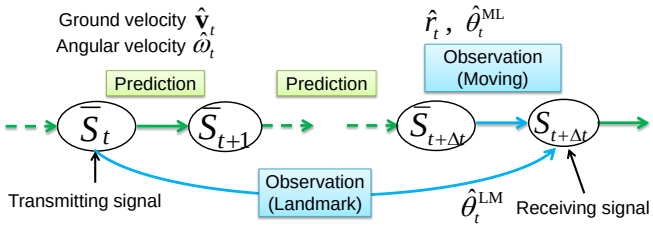

Figure 2 Timeline of state estimation process.

This paper assumes two AUVs (one moving and the other stationary and acting as a landmark). The moving AUV estimates the states using the particle filter. The particle filter represents the probability density function of both AUVs' states $p(X)$ at time *t* by a set of particles S_t as follows:

$$p(X) \cong S_t = \{\mathbf{s}_t^i \mid i = 1, \cdots n\} \tag{1}$$

$$\mathbf{s}_t^i = \left[x_t^{\mathrm{M}i}\ y_t^{\mathrm{M}i}\ \psi_t^{\mathrm{M}i}\ x_t^{\mathrm{L}i}\ y_t^{\mathrm{L}i}\ \psi_t^{\mathrm{L}i}\right]^{\mathrm{T}} \tag{2}$$

$$\mathbf{x}_t^{\mathrm{M}i} = \left[x_t^{\mathrm{M}i}\ y_t^{\mathrm{M}i}\right]^{\mathrm{T}} \tag{3}$$

$$\mathbf{x}_t^{\mathrm{L}i} = \left[x_t^{\mathrm{L}i}\ y_t^{\mathrm{L}i}\right]^{\mathrm{T}} \tag{4}$$

where $\mathbf{s}_t^i$ is the *i*th particle and *n* is the number of particles. The suffixes M and L denote "moving" and "landmark," respectively. The prediction phase updates the states from the ground velocity $\hat{\mathbf{v}}_{\mathrm{t}}^{\mathrm{M}}$ and the heading angular velocity $\hat{\omega}_t^{\mathrm{M}}$, as discussed above. Hat denotes measurements data. Thus, the state of the moving AUV is updated as

$$\mathbf{x}_{t+1}^{\mathrm{M}i} = \mathbf{x}_t^{\mathrm{M}i} + \mathbf{R}\left(\psi_t^{\mathrm{M}i}\right)\mathbf{v}_t^{\mathrm{M}i}\Delta t \tag{5}$$

$$\mathbf{v}_t^{\mathrm{M}i} \sim N\left(\hat{\mathbf{v}}_t^{\mathrm{M}}, \left(\sigma_{\mathbf{v}t}^{\mathrm{M}}\right)^2\right) \tag{6}$$

$$\psi_{t+1}^{\mathrm{M}i} = \psi_t^{\mathrm{M}i} + \omega_t^{\mathrm{M}i}\Delta t \tag{7}$$

$$\omega_t^{\mathrm{M}i} \sim N\left(\hat{\omega}_t^{\mathrm{M}}, \left(\sigma_{\omega t}^{\mathrm{M}}\right)^2\right) \tag{8}$$

where $\mathbf{R}$ is a rotation matrix. $\sigma_{\mathbf{v}t}^{\mathrm{M}}$ and $\sigma_{\omega t}^{\mathrm{M}}$ are standard deviations of the ground velocity and angular velocity, respectively. $N\left(\mu, \sigma^2\right)$ is a Gaussian sampling with mean μ and variance σ^2. Since the landmark AUV is stationary on the seafloor, its ground velocity and heading angular velocity are assumed as 0.

Observation is implemented in the second phase. If the measurements of relative direction and distance between the two AUVs are successful, they are used by the moving AUV to update the particles.

The likelihood of each particle is given by

$$w_t^i = L\left(\mathbf{s}_t^i\right) = L_{\mathrm{ML}}\left(\mathbf{s}_t^i\right) \cdot L_{\mathrm{LM}}\left(\mathbf{s}_t^i\right) \tag{9}$$

where L_{ML} and L_{LM} are the likelihoods estimated from measurements collected by the moving and landmark AUVs, respectively. w_t^i denotes the weight of the *i*th particle.

When no positioning measurements are obtained, the weight is assigned as 1, and the likelihood value remains unchanged.

L_{ML} is obtained as follows. The observation data are the relative distance $\hat{r}_t$ and the direction $\hat{\theta}_t^{\mathrm{ML}}$ measured by the moving AUV. The offsets in distance and direction, calculated from states at both time *t* (time of signal transmission) and time $t + \Delta t$ (time of signal reception), are given by

$$\Delta r_t^i = \left| \frac{\left|\mathbf{x}_{t+\Delta t}^{\mathrm{L}i} - \mathbf{x}_{t+\Delta t}^{\mathrm{M}i}\right| + \left|\mathbf{x}_t^{\mathrm{L}i} - \mathbf{x}_t^{\mathrm{M}i}\right|}{2} - \hat{r}_t \right| \quad (10)$$

$$\Delta\theta_t^{\mathrm{ML}i} = \left| \arg\left(\mathbf{x}_{t+\Delta t}^{\mathrm{L}i} - \mathbf{x}_{t+\Delta t}^{\mathrm{M}i}\right) - \left(\psi_{t+\Delta t}^{\mathrm{M}i} + \hat{\theta}_t^{\mathrm{ML}}\right) \right| \quad (11)$$

where the terms are defined in Figure 3. The likelihood $L_{\mathrm{ML}}\left(\mathbf{s}_t^i\right)$ is then calculated as follows:

$$L_{\mathrm{LM}}\left(\mathbf{s}_t^i\right) = \begin{cases} \text{if } \left(\Delta r_t^i < k_r\sigma_r\right) \cap \left(\Delta\theta_t^{\mathrm{ML}i} < k_\theta^{\mathrm{M}}\sigma_\theta^{\mathrm{M}}\right) \\ \quad \left\{\exp\left(\frac{k_r^{\,2}}{2} + \frac{-\left(\Delta r_t^i\right)^2}{2\sigma_r^{\,2}}\right)\right\} \cdot \left\{\exp\left(\frac{\left(k_\theta^{\mathrm{M}}\right)^2}{2} + \frac{-\left(\Delta\theta_t^{\mathrm{ML}i}\right)^2}{2\left(\sigma_\theta^{\mathrm{M}}\right)^2}\right)\right\} \\ \text{else} \\ \quad 1 \end{cases} \quad (12)$$

σ_r and $\sigma_\theta^{\mathrm{M}}$ are the standard deviations of the distance and direction, respectively, measured by the moving AUV. Gaussian errors are assumed in the measurements. The parameters k_r and k_θ^{M} prevent extreme fallout of the likelihood when outliers enter the measurements [6]. The terms $k_r^{\,2}/2$ and $\left(k_\theta^{\mathrm{M}}\right)^2/2$ in the exponential functions smooth the output at the boundaries.

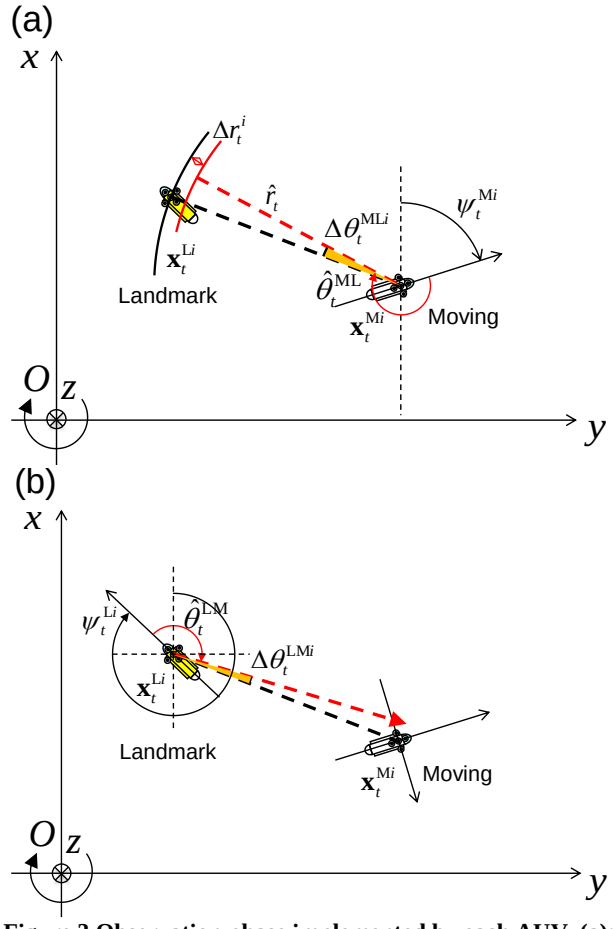

Figure 3 Observation phase implemented by each AUV. (a): Positioning measurements determined by the moving AUV. (b): Positioning measurements determined by the landmark AUV.

Similarly, $L_{\mathrm{LM}}\left(\mathbf{s}_t^i\right)$ is calculated from the relative direction $\hat{\theta}_t^{\mathrm{LM}}$ measured by the landmark AUV as

$$\Delta\theta_t^{\mathrm{LM}i} = \left| \arg\left(\mathbf{x}_t^{\mathrm{M}i} - \mathbf{x}_t^{\mathrm{L}i}\right) - \left(\psi_t^{\mathrm{L}i} + \hat{\theta}_t^{\mathrm{LM}}\right) \right| \quad (13)$$

$$L_{\mathrm{LM}}\left(\mathbf{s}_t^i\right) = \begin{cases} \text{if } \left(\Delta\theta_t^{\mathrm{LM}i} < k_\theta^{\mathrm{L}}\sigma_\theta^{\mathrm{L}}\right) \\ \quad \exp\left(\frac{\left(k_\theta^{\mathrm{L}}\right)^2}{2} + \frac{-\left(\Delta\theta_t^{\mathrm{LM}i}\right)^2}{2\left(\sigma_\theta^{\mathrm{L}}\right)^2}\right) \\ \text{else} \\ \quad 1 \end{cases} \quad (14)$$

Each particle is weighted by the weight function **(9)**, and resampled to determine S_{t+1}.

Although the particle filter ensures robustness to sensor noises during state estimation, it offers no protection against positioning errors, which may cause incorrect convergence of the particles. This problem is significant because it degrades the states of the landmark AUV during the landmark role exchange. Such localization failure, known as "robot kidnapping," can be resolved by adding random particles based on the probability of sensor measurements [12]. Here, the average likelihood of the state $\overline{L(S_t)}$ is monitored and localization failure is corrected by adding new particles (particle reconstruction). The average likelihood is defined as

$$\overline{L(S_t)} = \frac{1}{n}\sum_{i=1}^{n} L\left(\mathbf{s}_t^i\right) \quad (15)$$

Localization failure is indicated by a marked drop in the average likelihood. In the absence of errors, the likelihood is defined as

$$L_{\max} = L_{\mathrm{ML}} \cdot L_{\mathrm{LM}} \quad (16)$$

$$L_{\mathrm{ML}} = \exp\left(\frac{k_r^{\,2} + \left(k_\theta^{\mathrm{M}}\right)^2}{2}\right) \quad (17)$$

$$L_{\mathrm{LM}} = \exp\left(\frac{\left(k_\theta^{\mathrm{L}}\right)^2}{2}\right) \quad (18)$$

In the absence of valid positioning measurements, both likelihood (**(17)** and **(18)**) are set to 1. The average likelihood also decreases when outliers enter the measurements. To distinguish localization failure from outliers, the likelihood transit is monitored. Decreased likelihood is attributed to localization failure when $\overline{L(S_t)} < k \cdot L_{\max} \cap \overline{L(S_{t-\Delta t})} < k \cdot L_{\max} \cap \cdots \cap \overline{L(S_{t-a\Delta t})} < k \cdot L_{\max}$, where Δt is the time interval between positioning measurements, and k is an arbitrary multiplication threshold that decides whether likelihood decreases. a is an arbitrary

trial number that determines the time of likelihood monitoring. These arbitrary values are determined from the results of sea experiments (Section IV).

Particles are selected and replaced by new particles in order of ascending likelihood. The number of new particles is determined by

$$n_{\text{new}} = \left\lfloor n \cdot r \left\{ 1.0 - \frac{\log\left(\overline{L(S_t)}\right)}{\log\left(L_{\max}\right)} \right\} \right\rfloor \quad \textbf{(19)}$$

$\lfloor x \rfloor$ denotes the largest integer not exceeding x (the floor function). The logarithmic function prevents extreme fallout of the likelihood caused by the exponential function. To prevent exchange of the entire particle set, the number of replacements is limited to 100r %. At least a measurements are required between one particle reconstruction and the next.

A new ith particle is determined from the states of the landmark AUV and positioning measurements. First, the ith particle's positioning measurements are sampled from a Gaussian distribution with mean μ and variance σ^2 (**(20)**–**(22)**), where μ and σ^2 are the raw value and the performance of the positioning measurements, respectively. The ith new state $\hat{\mathbf{s}}_t^{\mathrm{M}i} = \left[\hat{x}_t^{\mathrm{M}i}\ \hat{y}_t^{\mathrm{M}i}\ \hat{\psi}_t^{\mathrm{M}i}\right]^{\mathrm{T}}$ is calculated from **(23)**–**(25)**. In particle reconstruction, only the states of the moving AUV are revised. The landmark states are unchanged.

$$r_t^i \sim N\left(\hat{r}, \left(\sigma_r\right)^2\right) \quad \textbf{(20)}$$

$$\theta_t^{\mathrm{ML}i} \sim N\left(\hat{\theta}_t^{\mathrm{ML}}, \left(\sigma_\theta^{\mathrm{M}}\right)^2\right) \quad \textbf{(21)}$$

$$\theta_t^{\mathrm{LM}i} \sim N\left(\hat{\theta}_t^{\mathrm{LM}}, \left(\sigma_\theta^{\mathrm{L}}\right)^2\right) \quad \textbf{(22)}$$

$$\hat{x}_t^{\mathrm{M}i} = x_t^{\mathrm{L}i} + r_t^i \cos(\psi_t^{\mathrm{L}i} + \theta_t^{\mathrm{LM}i}) \quad \textbf{(23)}$$

$$\hat{y}_t^{\mathrm{M}i} = y_t^{\mathrm{L}i} + r_t^i \sin(\psi_t^{\mathrm{L}i} + \theta_t^{\mathrm{LM}i}) \quad \textbf{(24)}$$

$$\hat{\psi}_t^{\mathrm{M}i} = \psi_t^{\mathrm{L}i} + \theta_t^{\mathrm{LM}i} - \theta_t^{\mathrm{ML}i} - \pi \quad \textbf{(25)}$$

D. State Compression

When AUVs exchange the landmark role, they share the distributions of the states estimated by the moving AUV. As mentioned in Section IIC, the state of each particle is composed of six parameters $\mathbf{s}_t^i = \left[x_t^{\mathrm{M}i}\ y_t^{\mathrm{M}i}\ \psi_t^{\mathrm{M}i}\ x_t^{\mathrm{L}i}\ y_t^{\mathrm{L}i}\ \psi_t^{\mathrm{L}i}\right]^{\mathrm{T}}$.

If the number of particles exceeds a few hundred, the data size becomes too large for state sharing in the underwater environment, where the rates of acoustical communications are typically low. To overcome this problem, the previously moving AUV (AUV A) compresses the estimated states before transmitting the information to the next moving AUV (AUV B). The procedure of the state sharing is as follows:

1) A lands on the seafloor and measures the mutual acoustical positioning between itself and B to converge the state uncertainties.
2) To reduce the communication data size, A compresses the estimated states by "particle clustering" using a clustering method and a model selection method.
3) A transmits the compressed information regarding the estimated states to B.

The abovementioned "particle clustering" approximates the original states (particles) by a combined clustering and model selection approach. The data compression method is detailed in a previous paper [27].

III. Implementation

A. Acoustical Positioning and Communication System

The proposed method was implemented on a positioning and communication device named acoustical localization and communication (ALOC). A photograph of the device and the device specifications are presented in Figure 4 and Table 1, respectively. The ALOC, comprising one transmitter and four receivers, enables communication among multiple underwater vehicles. It also enables AUVs to calculate their relative positions from acoustical measurements using a short base line (SBL) technique. Transmitted waves constitute chirp signals (for relative positioning) and communication signals. The latter are transmitted using multiple-value frequency-shift keying at a data rate of 100 bits per second with a data size of 8 bytes. Transducers have both horizontally and vertically omnidirectional beam patterns. This system is suitable for the proposed navigation.

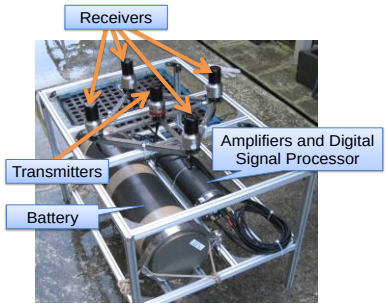

Figure 4 Positioning and Communication device ALOC [25].

Table 1
Specifications of ALOC

Positioning	chirp (22-28kHz), SBL
Communication	multiple-value FSK (23-26kHz) data rate: 100 bits per second (bps) data size (per signal): 8 bytes

B. Vehicles

The method is implemented in two AUVs; Tri-Dog 1 (TD) and Tri-TON 1 (TT). Both AUVs are hovering type AUVs with thrusters that can independently control surge, sway, heave, and yaw motions [28], [29]. A hovering type AUV can maintain a constant altitude from the seafloor and is

therefore suitable for detailed seafloor observation. Photographs and specifications of the AUVs are shown in Figure 5 & Figure 6 and TABLE 2 & TABLE 3, respectively. Ground velocity is measured by a DVL and yaw angular velocity is measured by a one-axis FOG. The ALOC is mounted on the top center of the AUV. The AUV is also equipped with a landing foot for landing on the seafloor. The performances of the DVL and FOG (navigation sensors) and the ALOC (positioning sensor) are summarized in Figure 9 plots the real-time horizontal trajectories and the positioning measurements obtained from both AUVs. Blue and red lines (dots) show the trajectories (particles) of TD and TT, respectively. The left and right panels, respectively, show the positioning measurements of the moving and landmark AUVs. These measurements were derived from the relative distance measured by the moving AUV and the relative direction measured by both AUVs. The positioning measurements of TD and TT are plotted in black and green, respectively. This figure shows how the positioning measurements and the estimated trajectories deviate over time. Note that the incorrect particle convergence occurred in Figure 9(b). This indicates that TD could not resolve the offsets between positioning measurements and states; consequently, its trajectory was misled, and the localization failed.

Figure 10 shows the positional offsets and likelihood of the positioning measurements. Offsets are calculated from **(10)**, **(11)**, and **(13)**, while likelihood is calculated from **(12)** and **(14)**. Immediately prior to landmark role exchange, the positioning offsets increased and the likelihood decreased. Eventually, these offsets accumulated until they became non-negligible.

To resolve this problem, particle reconstruction was adopted in the post-processing simulations. In Figure 10, localization failure is assumed when the likelihood of each measurement is below 85% of maximum likelihood. Since the total likelihood is calculated from three measurements, $\boldsymbol{k}$ was calculated as $0.85 \times 0.85 \times 0.85 \approx 0.6$. Approximately 15 positioning measurements were taken while the AUV assumed the moving role; therefore $\boldsymbol{a}$ was set to 2. To avoid the exchange of all particles in the reconstruction, $\boldsymbol{r}$ was set to 0.5.

C. Post-processing Simulation

The performance of the proposed method was evaluated in post-processing simulations using the experimental results, namely, the ground velocity, angular velocity, and relative positioning measurements. From these results, the simulations recalculated the horizontal position and the heading angle. The simulated performances of the proposed method were compared with those of dead reckoning. In dead reckoning, the AUVs estimate the state solely from the ground and angular velocities. The performance of the sensors is summarized in **Error! Not a valid bookmark self-reference.**. Outlier thresholds (k_r, k_θ^{M}, k_θ^{L}) were set to 3 to regard positioning measurements which have offsets more than three sigma (99 % error range) as outliers. To enhance the estimation accuracy, the number of particles was set to 3000 (300 in the sea experiments).

TABLE 4 PERFORMANCE OF THE SENSORS

DVL	$\sigma_v = 0.00084 + 0.038\sqrt{\lvert v \rvert}$ [m/s] $(0.05 \le \lvert v \rvert \le 0.5)$
FOG	$\sigma_\omega = 0.0745$ [deg/s]
Positioning(distance)	$\sigma_r = 0.66$ [m]
Positioning(direction from moving AUV)	$\sigma_\theta^{\mathrm{ML}} = 6.0$ [deg]
Positioning(direction from landmark AUV)	$\sigma_\theta^{\mathrm{LM}} = 1.0$ [deg]
Outlier threshold k_r , k_θ^{M} , k_θ^{L}	3.0

Figure 11 plots the simulated horizontal trajectories and positioning measurements of the AUVs. Blue and red lines (dots) show the trajectories (particles) of TD and TT, respectively. The upper panels show the positioning measurements derived from the relative distance and direction by the landmark AUV. Left and right panels show the results estimated by dead reckoning and the proposed method, respectively. The positioning measurements more closely match the trajectories in the proposed method than in the dead reckoning case. The lower panels show the positioning measurements obtained from relative distance and direction by the moving AUV. Again, the left and right panels show the positioning results of dead reckoning and the proposed method, respectively, and the trajectories are better matched by the proposed method than by dead reckoning. Therefore, we infer that particles converge correctly in the proposed method, but gradually diverge in dead reckoning. As evidenced in the upper left panel of Figure 11, the positioning measurements from TT are confined to the particle distributions, indicating that the AUVs correctly estimate their states from positioning measurements.

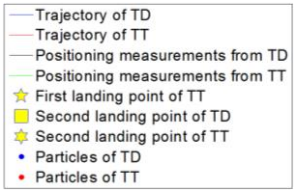

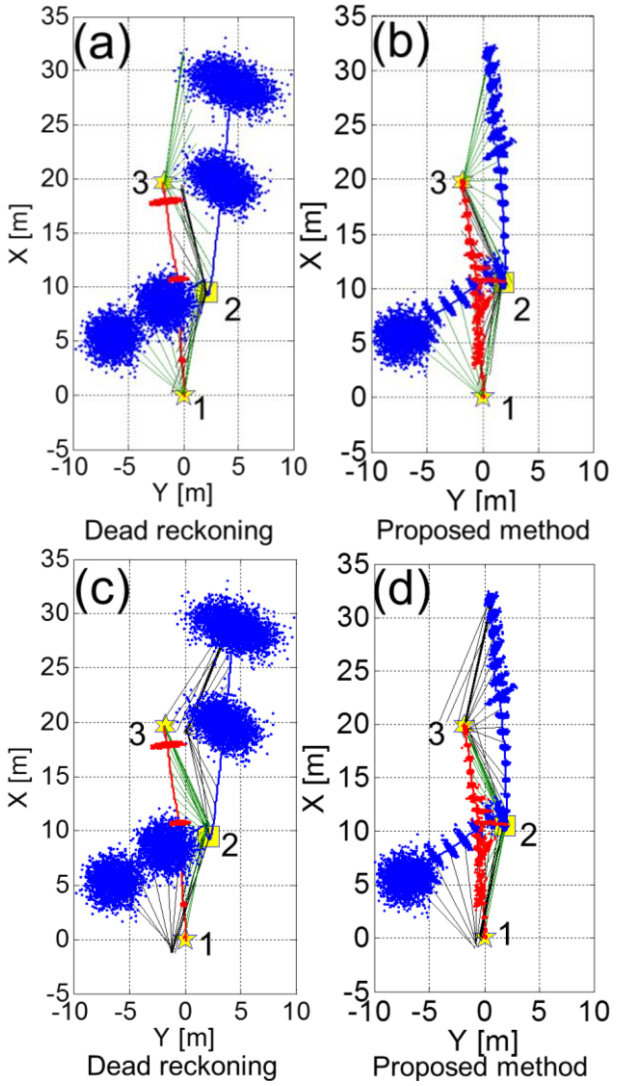

Figure 11 Horizontal trajectories of the AUVs estimated from post-processing simulation and positioning measurements of the landmark AUV ((a), (b)) and the moving AUV ((c), (d)).

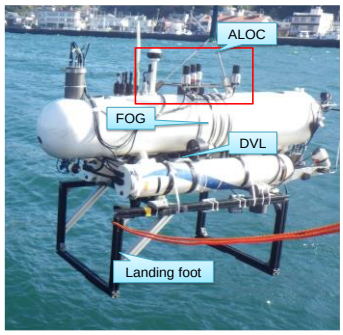

Figure 5 AUV Tri-Dog 1.

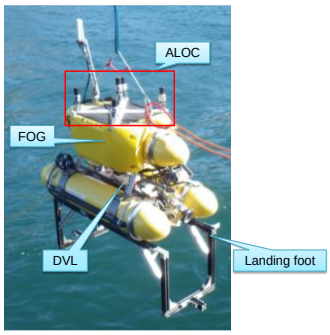

Figure 6 AUV Tri-TON 1.

TABLE 2
SPECIFICATIONS OF TRI-DOG 1

Length	2.0 m
Width	0.6 m
Height	1.4 m (with the landing foot)
Weight	200 kg (In air) 1.5 kg(In water)
Max. depth	110 m
Endurance	4 hours
Thrusters	100 W × 6
Sensors	Doppler Velocity Log (DVL) One-axis Fiber Optic Gyro (FOG) Attitude sensor Pressure sensor Acoustic range sensor × 6 Forward camera Downward camera ALOC

TABLE 3
SPECIFICATIONS OF TRI-TON 1

Length	1.4 m
Width	0.76 m
Height	1.8 m (with the landing foot)
Max. depth	800 m
Weight	230 kg (In air) 1.5 kg(In water)
Endurance	8 hours
Sensors	Doppler Velocity Log (DVL) One-axis Fiber Optic Gyro (FOG) Attitude sensor Pressure sensor Forward camera Downward camera ALOC

IV. SEA EXPERIMENTS

As mentioned above, the proposed method was implemented in AUV Tri-Dog 1 (TD) and AUV Tri-TON 1 (TT). Sea trials were conducted in November 2013. The depth of the experimental sites was approximately 30 m.

A. Deployment Procedure

The following deployment procedure was adopted.

1) The AUV initially assigned the landmark role (assumed as TT) is first deployed. TT is manually guided to the deployment point on the sea surface, where it dives toward the seafloor to act as the landmark AUV. After landing on the seafloor, TT remains stationary, awaiting the moving AUV.
2) The AUV initially assigned the moving role (assumed as TD) is then deployed. TD is manually guided to its deployment points 10 m distant from TT on the sea surface, and then begins diving.
3) TD approaches and lands on the seafloor.
4) After landing on the seafloor, TD begins searching for TT using the ALOC system.
5) After finding TT, TD begins a seafloor observation relative to TT. The reference surge velocity is retained at 0.15 m/s. The sampling frequency of the navigation sensors is 5 Hz and the positioning interval is 10 s. The observation route is preplanned and based on the first landing point of TT.
6) When TD reaches the predefined point where the AUVs switch roles, it lands on the seafloor to act as the landmark.

7) Using ALOC, TD transmits the compressed information of the estimated states to TT.
8) TT starts moving and estimates the states using the information received from TD.
9) TT lands on the seafloor at predefined points and transmits compressed information of the states to TD.
10) Procedures 5 to 9 are repeated until mission timeout.

Global positions of the AUVs were not measured in this experiment. The global trajectories can be obtained by combining relative trajectories of the AUVs with the first landed positions of the AUVs globally localized by ultra short base line (USBL) with a GPS receiver.

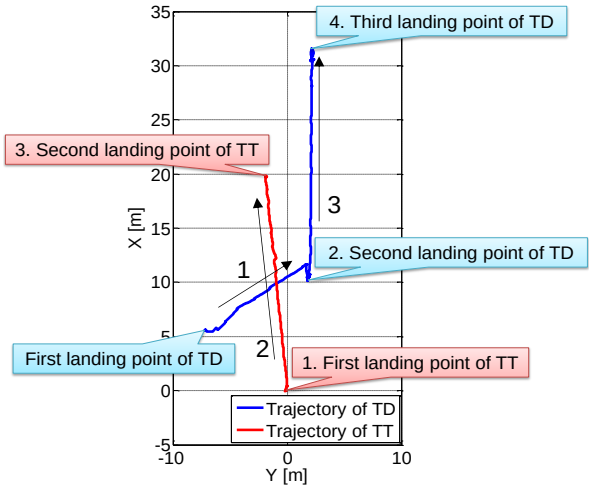

Figure 7 Horizontal trajectories of two AUVs.

B. *Experimental Results*

Figure 7 plots the horizontal trajectories of the two AUVs, indicating the roles of the AUVs and the procedural events. The blue and red paths show the trajectories of TD and TT, respectively. At its first landing point, TT remained stationary on the seafloor and awaited the arrival of TD. As TD arrived at its first landing point, it located TT, and then moved to its second landing point (event 1 in Figure 7). TD dived to the seafloor, and then transmitted compressed information about the states to TT. After receiving information, TT started moving to the second landing point (event 2), and the process repeated.

Figure 8 shows the horizontal ground velocities of both AUVs during events 1–3 in Figure 7. From this figure, we observe that while one AUV was moving the other remained stationary. During the first 100 s, TD moved from the first to the second landing point (event 1). From 100–300 s, TD transmitted compressed information to TT. During the next 150 s (300–450 s), TT moved from the first to the second landing point (event 2). Clearly from these results, the two AUVs alternately became the landmark.

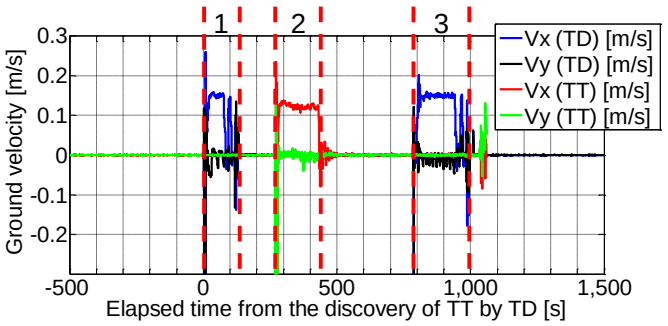

Figure 8 Horizontal ground velocities of two cooperating AUVs.

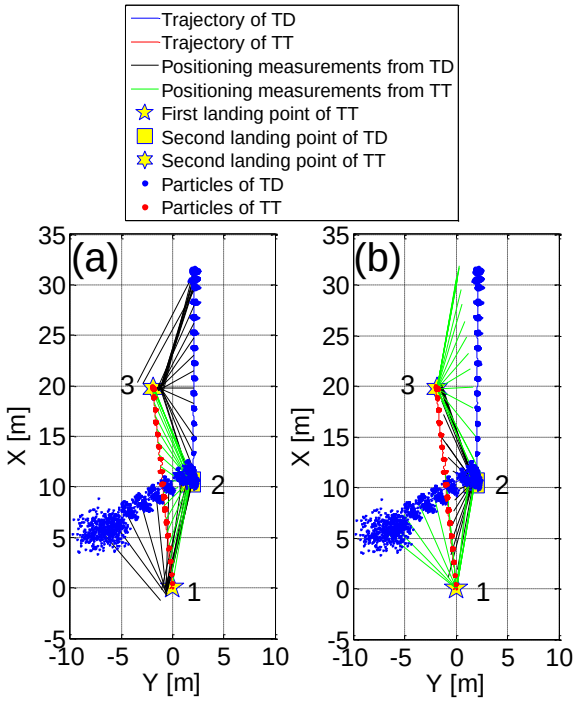

Figure 9 Horizontal trajectories of two AUVs estimated in sea trials and positioning measurements: (a) from the moving AUV; (b) from the landmark AUV.

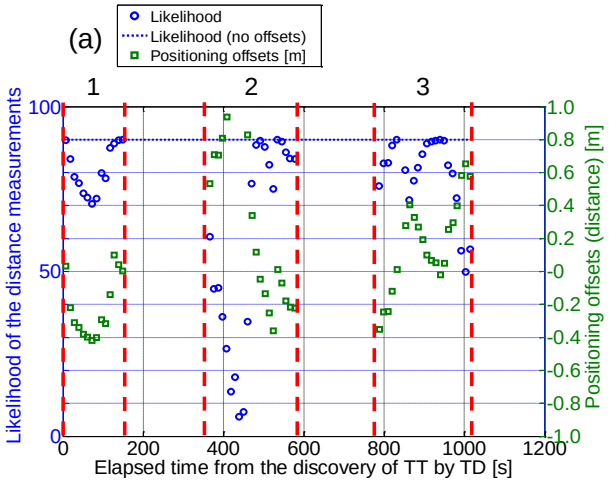

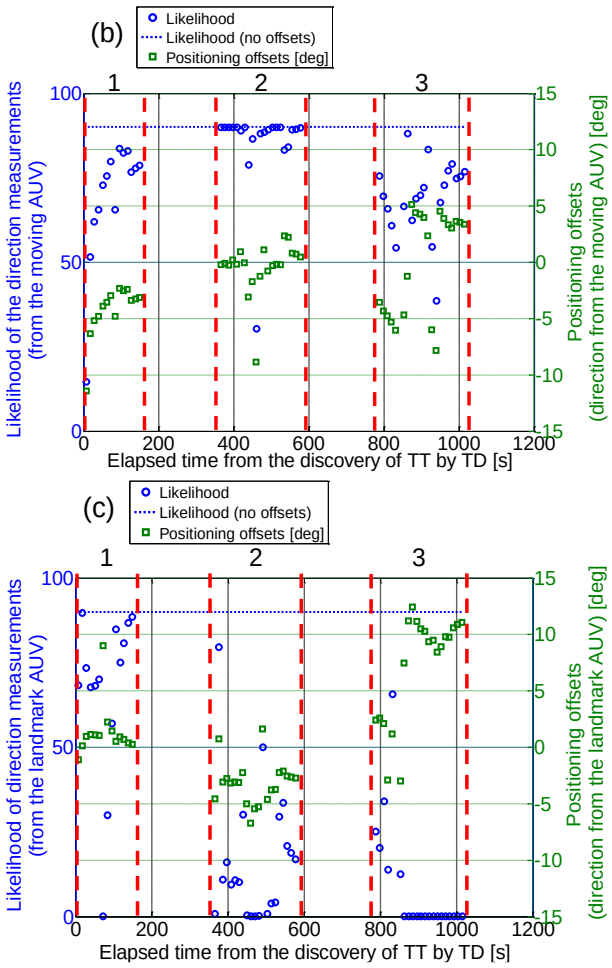

Figure 10 Positional offsets and likelihood in sea experiments of (a) distance measurements, (b) directional measurements from the moving AUV, and (c) directional measurements from the landmark AUV.

Figure 9 plots the real-time horizontal trajectories and the positioning measurements obtained from both AUVs. Blue and red lines (dots) show the trajectories (particles) of TD and TT, respectively. The left and right panels, respectively, show the positioning measurements of the moving and landmark AUVs. These measurements were derived from the relative distance measured by the moving AUV and the relative direction measured by both AUVs. The positioning measurements of TD and TT are plotted in black and green, respectively. This figure shows how the positioning measurements and the estimated trajectories deviate over time. Note that the incorrect particle convergence occurred in Figure 9(b). This indicates that TD could not resolve the offsets between positioning measurements and states; consequently, its trajectory was misled, and the localization failed.

Figure 10 shows the positional offsets and likelihood of the positioning measurements. Offsets are calculated from **(10)**, **(11)**, and **(13)**, while likelihood is calculated from **(12)** and **(14)**. Immediately prior to landmark role exchange, the positioning offsets increased and the likelihood decreased. Eventually, these offsets accumulated until they became non-negligible.

To resolve this problem, particle reconstruction was adopted in the post-processing simulations. In Figure 10, localization failure is assumed when the likelihood of each measurement is below 85% of maximum likelihood. Since the total likelihood is calculated from three measurements, $\boldsymbol{k}$ was calculated as $0.85 \times 0.85 \times 0.85 \approx 0.6$. Approximately 15 positioning measurements were taken while the AUV assumed the moving role; therefore $\boldsymbol{a}$ was set to 2. To avoid the exchange of all particles in the reconstruction, $\boldsymbol{r}$ was set to 0.5.

C. Post-processing Simulation

The performance of the proposed method was evaluated in post-processing simulations using the experimental results, namely, the ground velocity, angular velocity, and relative positioning measurements. From these results, the simulations recalculated the horizontal position and the heading angle. The simulated performances of the proposed method were compared with those of dead reckoning. In dead reckoning, the AUVs estimate the state solely from the ground and angular velocities. The performance of the sensors is summarized in **Error! Not a valid bookmark self-reference.**. Outlier thresholds (k_r, k_θ^{M}, k_θ^{L}) were set to 3 to regard positioning measurements which have offsets more than three sigma (99 % error range) as outliers. To enhance the estimation accuracy, the number of particles was set to 3000 (300 in the sea experiments).

TABLE 4 PERFORMANCE OF THE SENSORS

DVL	$\sigma_v = 0.00084 + 0.038\sqrt{\lvert v \rvert}$ [m/s] $(0.05 \le \lvert v \rvert \le 0.5)$
FOG	$\sigma_\omega = 0.0745$ [deg/s]
Positioning(distance)	$\sigma_r = 0.66$ [m]
Positioning(direction from moving AUV)	$\sigma_\theta^{\mathrm{ML}} = 6.0$ [deg]
Positioning(direction from landmark AUV)	$\sigma_\theta^{\mathrm{LM}} = 1.0$ [deg]
Outlier threshold k_r, k_θ^{M}, k_θ^{L}	3.0

Figure 11 plots the simulated horizontal trajectories and positioning measurements of the AUVs. Blue and red lines (dots) show the trajectories (particles) of TD and TT, respectively. The upper panels show the positioning measurements derived from the relative distance and direction by the landmark AUV. Left and right panels show the results estimated by dead reckoning and the proposed method, respectively. The positioning measurements more closely match the trajectories in the proposed method than in the dead reckoning case. The lower panels show the positioning measurements obtained from relative distance and direction by the moving AUV. Again, the left and right panels show the positioning results of dead reckoning and the proposed method, respectively, and the trajectories are better matched by the proposed method than by dead reckoning. Therefore, we infer that particles converge correctly in the proposed method, but gradually diverge in dead reckoning. As evidenced in the upper left panel of Figure 11, the positioning measurements from TT are confined to the particle distributions, indicating that the AUVs correctly estimate their states from positioning measurements.

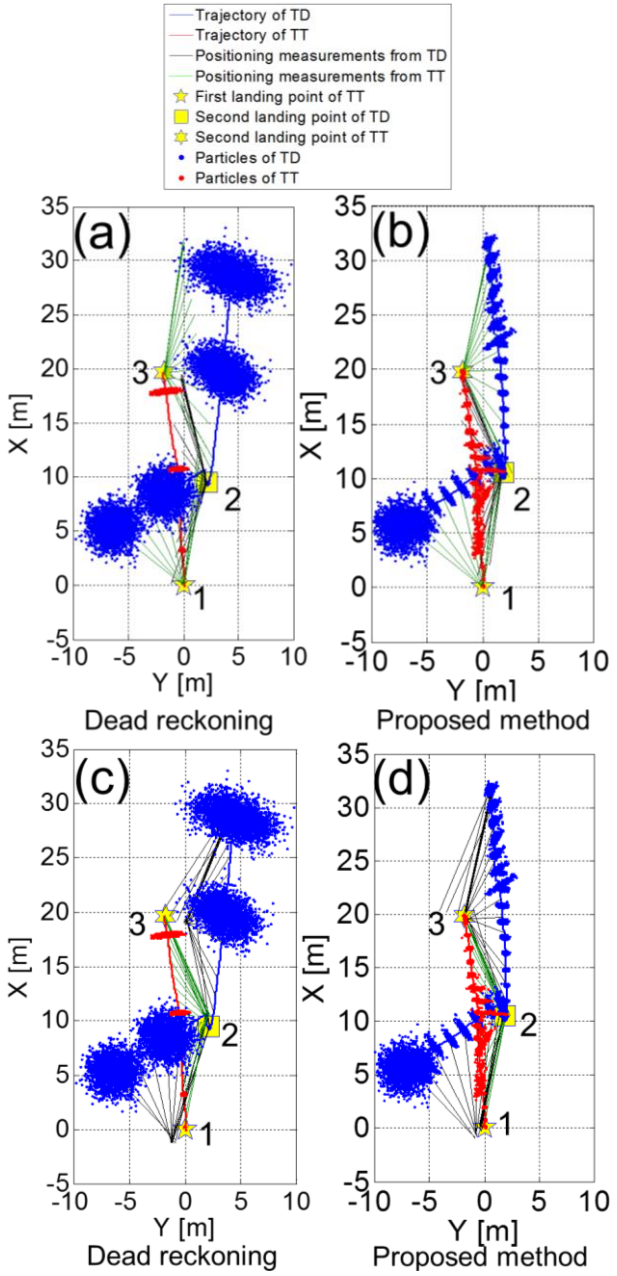

Figure 11 Horizontal trajectories of the AUVs estimated from post-processing simulation and positioning measurements of the landmark AUV ((a), (b)) and the moving AUV ((c), (d)).

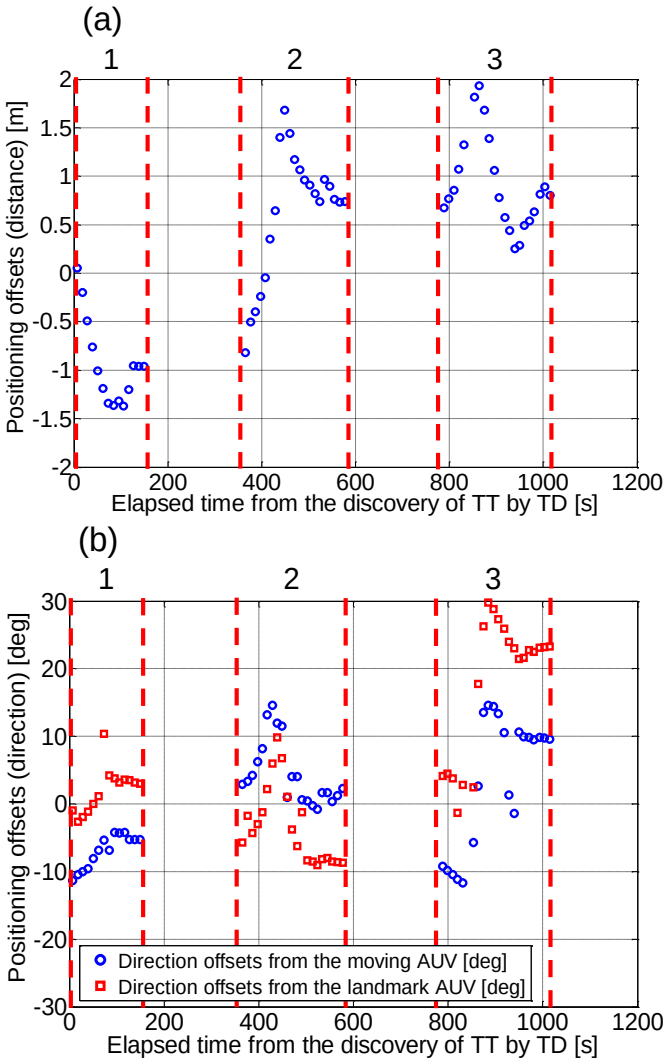

Figure 12 Positioning offsets in the dead reckoning case. (a) Results of distance measurements; (b) results of direction measurements.

Figure 12 shows the positioning offsets computed by dead reckoning. Top and bottom panels show the results of distance and directional measurements, respectively. The offsets exceed those obtained in the sea experiments. In dead reckoning, the heading errors were sufficiently high to contribute to positioning errors. As shown in Figure 11(a), the estimated trajectory of TD was misled by dead reckoning.

Figure 13 shows the positioning offsets and likelihood obtained by the proposed method. Each plot is constructed similar to Figure 10. From this figure, we find that, immediately prior to landmark role exchange, the positioning offsets are smaller in the simulations than in the sea experiments. The likelihood is almost identical to those of the offset-free case. Particle reconstruction enables the AUVs to navigate and exchange the landmark role without expanding their estimation errors. Clearly, the positioning offsets are reduced from those of dead reckoning.

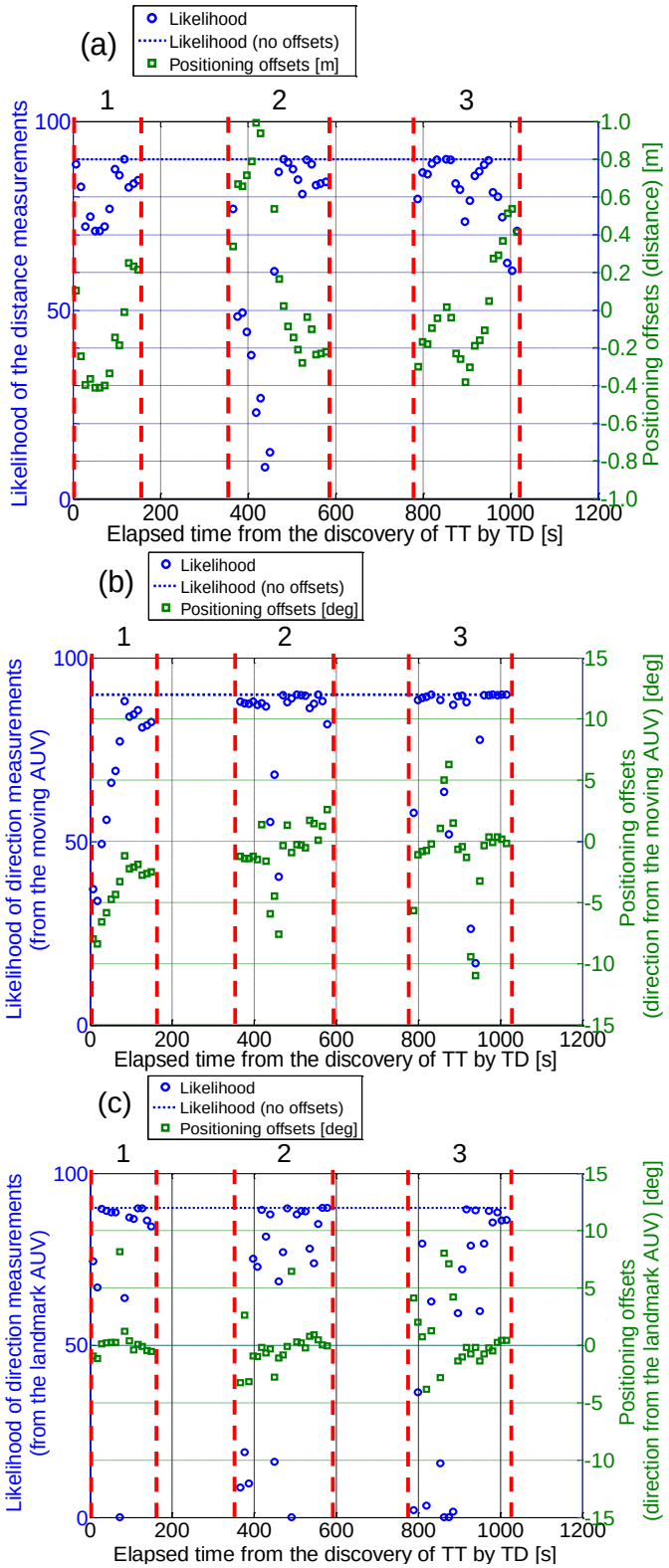

Figure 13 Positioning offsets and likelihood of positioning measurements in post-processing simulations of the proposed method. (a) Results of distance measurements; (b) results of direction measurements from the moving AUV; (c) results of direction measurements from the landmark AUV.

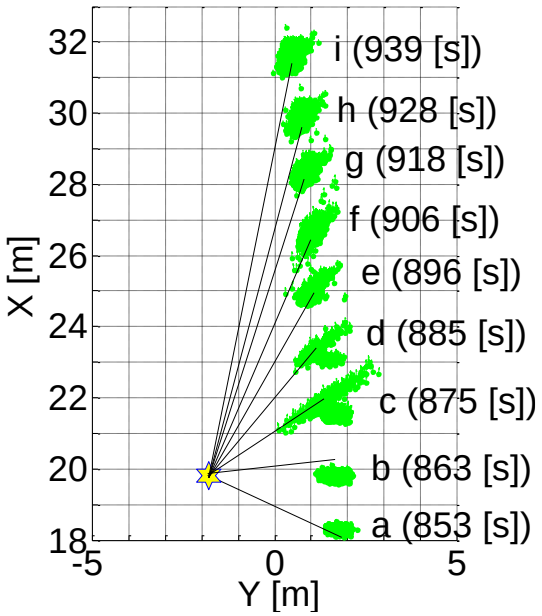

Figure 14 Particles and positioning measurements obtained from the landmark AUV. Times of positioning measurements are also shown.

Figure 14 shows the particle locations during positioning measurements at specified times. Black lines indicate the positions measured by the landmark AUV.

Figure 15 enlarges the measured positions plotted in Figure 14. Because the positioning measurements are separated from the estimated states in (a)–(c), some particles are reconstructed based on the positioning measurements at 875 s (panel (c)). Both pre-existent and additional particles form new distributions, which converge as the measurements proceed. The positional measurements and particle distributions coincide at 939 s (panel (i)).

Here, the number of particles were set to 3000. The increasing number of the particles results in more computational resource. To validate the real-time ability of the algorithm, the processing speed of the simulation was examined by changing the number of particles. TABLE 5 SPECIFICATIONS OF THE COMPUTER USED FOR THE SIMULATIONS.

CPU	Intel Core i7 3.0 GHz
Memory	16.0 GB
System	64 bit
Operating system	Windows 8

shows the performance of the computer used for the simulations. Figure 16 shows the computational time for all simulation process (blue line) and state compression process for each role exchange (green line). Computational time of the state compression for 10,000 particles was about 20 s. When the state compression is performed, both AUVs are landed on the seafloor. It was acceptable processing time for the real-time ability. Figure 17 shows the processing speed rate against total navigation time (1024 s). As the number of particles increased, the computational time increased. The simulation for 3,000 particles was processed 10 times quickly as the actual navigation. It was enough processing speed for real-time navigation. The simulation for 10,000 particles was processed 5

times quickly as the actual navigation. It was also acceptable processing speed for real-time navigation. Thus, it was verified that the proposed algorithm have the ability to process in real-time.

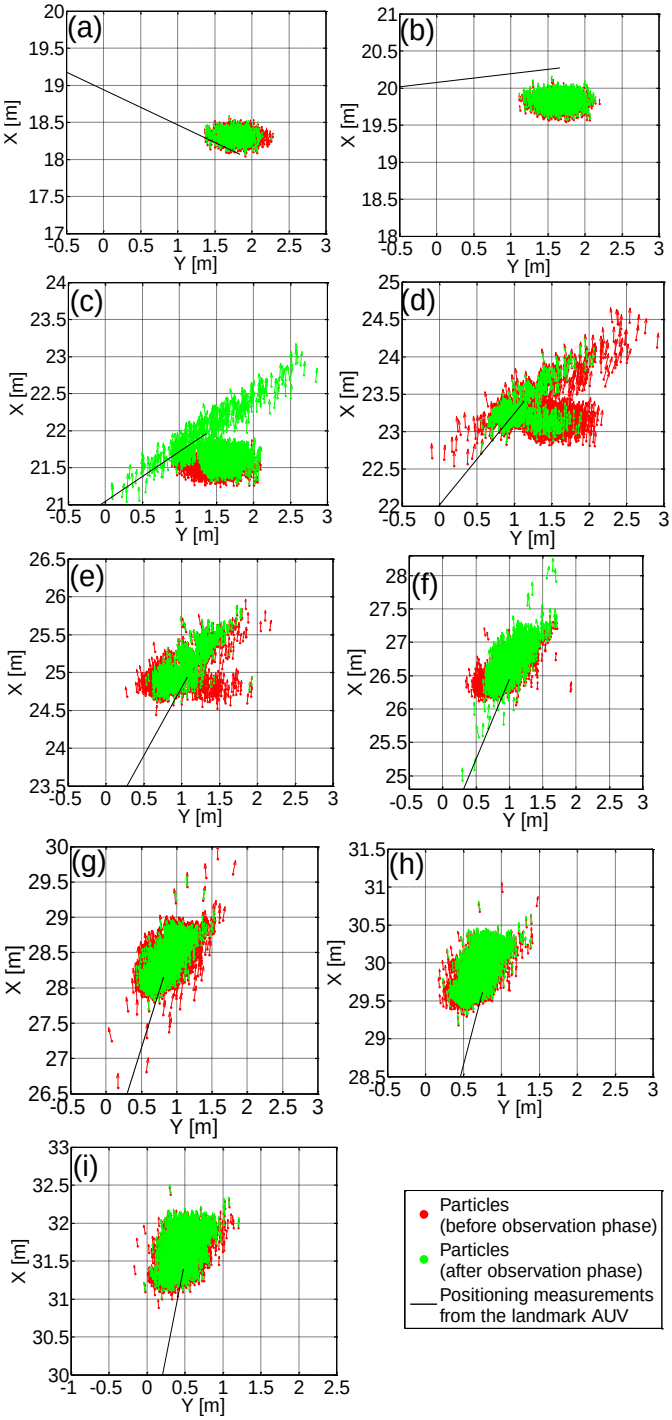

Figure 15 Enlargement of particle locations in Figure 14. Red and green dots denote particles immediately before and after detection in the observation phase, respectively. Labels (a)–(i) are defined in Figure 14.

TABLE 5
SPECIFICATIONS OF THE COMPUTER USED FOR THE SIMULATIONS.

CPU	Intel Core i7 3.0 GHz
Memory	16.0 GB
System	64 bit
Operating system	Windows 8

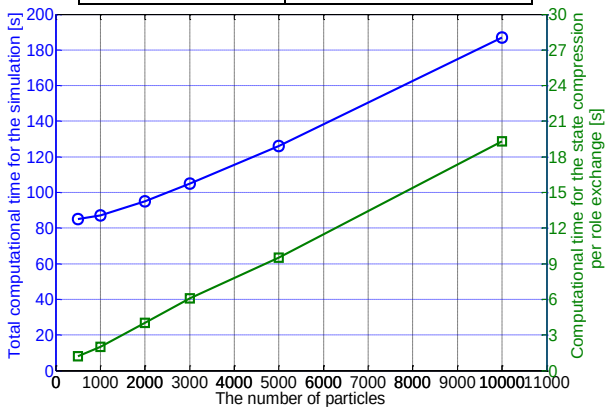

Figure 16 Computational time for the simulation and state compression process.

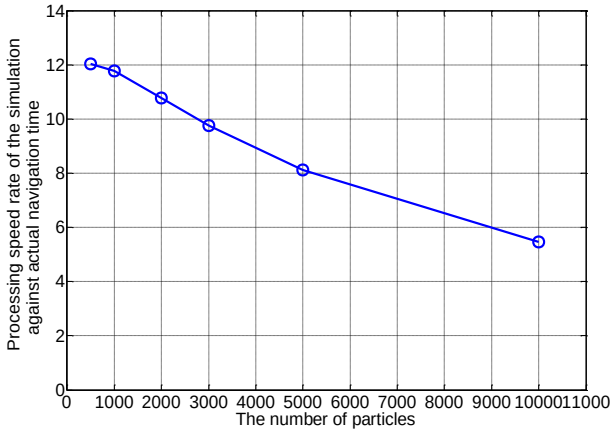

Figure 17 Processing speed rate of the simulation against actual navigation time.

In summary, by alternating the landmark role between two AUVs, the proposed method achieves small-drift navigation near the seafloor. Although the AUVs covered only 30 m in the present trial, repeated application of this process should realize long distance navigation.

V. CONCLUSIONS

In this paper, we reported sea experimental results of the cooperative navigation method of multiple AUVs and its performance. The method was implemented in two actual AUVs. Both AUVs successfully interchanged the landmark role, during which they remained stationary on the seafloor. In post-processing simulations, the proposed method demonstrated better performance than dead reckoning, and surpassed the results of sea experiments, by virtue of particle reconstruction. Positioning and heading errors were suppressed within 0.3 m and 1.0°, respectively. Thus, the proposed method meets the high-accuracy requirements of near seafloor mapping. Future work will focus on improving the proposed method and

mapping a wider area of the seafloor.

ACKNOWLEDGMENT

This work is also supported by Grant-in-Aid for JSPS (Japan Society for the Promotion of Science) Fellows Grant Number 12J06829. The authors thank all the staff of "OKI SEATEC" for their support at the experiments.

REFERENCES

[1] T. Matsuda, T. Maki, T. Sakamaki, and T. Ura, "Performance Analysis on a Navigation Method of Multiple AUVs for Wide Area Survey," Marine Technology Society Journal, vol. 46, no. 2, pp. 45–55, Mar. 2012, DOI: 10.4031/MTSJ.46.2.6.

[2] A. Budiyono, L. Chen, S. Wang, K. McDonald-Maier, and H. Hu, "Towards autonomous localization and mapping of AUVs: a survey," International Journal of Intelligent Unmanned Systems, vol.1, no.2, pp.97-120, 2013, DOI: 10.1108/20496421311330047.

[3] L. Paull, S. Saeedi, M. Seto, and H. Li, "AUV navigation and localization: A review," IEEE J. Ocean. Eng., vol.39, no.1, pp.131-149, 2014, 10.1109/JOE.2013.2278891.

[4] P. Sarhadi, A. Ranjbar Noei, and A. Khosravi, "L1 adaptive pitch control of an autonomous underwater vehicle," International Journal of Intelligent Unmanned Systems, vol.2, no.2, pp.107-120, 2014, DOI: 10.1108/IJIUS-12-2013-0025.

[5] T. Fujii, and T. Ura, "Development of motion control system for AUV using neural nets," Autonomous Underwater Vehicle Technology," AUV'90., Proceedings of AUV 90, pp.81-86, 1990, DOI: 10.1109/AUV.1990.110440.

[6] T. Maki, H. Kondo, T. Ura, and T. Sakamaki, "Positioning method for an AUV using a profiling sonar and passive acoustic landmarks for close-range observation of seafloors," in Proc. OCEANS Europe Conf., Jun. 2007, DOI: 10.1109/OCEANSE.2007.4302374.

[7] A. Caiti, A. Garulli, F. Livide, and D. Prattichizzo, "Localization of Autonomous Underwater Vehicles by Floating Acoustic Buoys : A Set-Membership Approach," IEEE J. Ocean. Eng., vol. 30, no. 1, pp. 140–152, Jan. 2005, DOI: 10.1109/JOE.2004.841432.

[8] T. Nakatani, T. Ura, T. Sakamaki, and J. Kojima, "Terrain based localization for pinpoint observation of deep seafloors," in Proc. OCEANS Europe Conf., May 2009, DOI: 10.1109/OCEANSE.2009.5278194.

[9] R. Kurazume, and S. Hirose, "An experimental study of a cooperative positioning system," Journal of Autonomous Robots, vol. 8, no. 1, pp. 43–52, Jan. 2000, DOI: 10.1023/A:1008988801987.

[10] I.M. Rekleitis, G. Dudek, and E.E. Milios, "Multi-Robot Cooperative Localization: A Study of Trade-offs Between Efficiency and Accuracy," in Proc. Intelligent Robots and System (IROS 2002), 2002, DOI: 10.1109/IRDS.2002.1041676.

[11] S. Tully, G. Kantor, and H. Choset, "Leap-frog path design for multi-robot cooperative localization," Field and Service Robotics, pp.307–317, 2010, DOI: 10.1007/978-3-642-13408-1_28.

[12] S. Thrun, W. Burgard, and D. Fox, Probabilistic robotics. Cambridge, Mass.: MIT Press, 2005, pp. 96-113.

[13] W. Burgard, M. Moors, C. Stachniss, and F.E. Schneider, "Coordinated multi-robot exploration," IEEE J. Robotics, vol. 21, no. 3, pp. 376–386, Jun., 2005, DOI: 10.1.1.59.4390.

[14] L. Techy, D.G. Schmale, and C.A. Woolsey, "Coordinated aerobiological sampling of a plant pathogen in the lower atmosphere using two autonomous unmanned aerial vehicles," Journal of Field Robotics, vol. 27, no. 3, pp. 335–343, May. 2010, DOI: 10.1002/rob.20335.

[15] C.E. Pippin, H. Christensen, and L. Weiss, "Dynamic, cooperative multi-robot patrolling with a team of UAVs," SPIE Defense, Security, and Sensing, pp.874103-874103, International Society for Optics and Photonics, 2013, DOI:10.1117/12.2014978.

[16] M. Bernard, K. Kondak, I. Maza, and A. Ollero, "Autonomous transportation and deployment with aerial robots for search and rescue missions," Journal of Field Robotics, vol.28, no.6, pp.914-931, 2011, DOI: 10.1002/rob.20401.

[17] C. Kunz, C. Murphy, R. Camilli, H. Singh, J. Bailey, R. Eustice, M. Jakuba, K. Nakamura, C. Roman, T. Sato, et al., "Deep sea underwater robotic exploration in the ice-covered arctic ocean with AUVs," in Proc. Intelligent Robots and System (IROS 2008), Sept. 2008, DOI: 10.1109/IROS.2008.4651097.

[18] G. Rui and M. Chitre, "Cooperative positioning using range-only measurements between two AUVs," in Proc. OCEANS Sydney Conf., May. 2010, DOI: 10.1109/OCEANSSYD.2010.5603615.

[19] G. Papadopoulos, M.F. Fallon, J.J. Leonard, and N.M. Patrikalakis, "Cooperative Localization of Marine Vehicles using Nonlinear State Estimation," in Proc. Intelligent Robots and System (IROS 2010), Oct., 2010, DOI: 10.1109/IROS.2010.5650250.

[20] Y. Jung, K. Lee, S. Lee, M. Choi, and B. Lee, "An efficient underwater coverage method for multi-AUV with sea current disturbances," International Journal of Control, Automation and Systems, vol. 7, no. 4, pp. 615–629, Aug. 2009, DOI: 10.1007/s12555-009-0412-4.

[21] R.M. Turner, S. Rode, and D. Gagne, "Distributed context-based organization and reorganization of multi-AUV systems," Journal of Unmanned System Technology, vol.2, no.1, pp.1-9, 2014.

[22] E. Fiorelli, N.E. Leonard, P. Bhatta, D.A. Paley, R. Bachmayer, and D.M. Fratantoni, "Multi-AUV control and adaptive sampling in Monterey Bay," IEEE J. Ocean. Eng., vol.31, no.4, pp.935-948, 2006, DOI: 10.1109/JOE.2006.880429.

[23] A. Bahr, M. Walter, and J. Leonard, "Consistent cooperative localization," in Proc. IEEE International Conference on Robotics and Automation (ICRA 2009), May., 2009, DOI: 10.1109/ROBOT.2009.5152859.

[24] T. Matsuda, T. Maki, Y. Sato, and T. Sakamaki, "Cooperative Navigation Method of Multiple Autonomous Underwater Vehicles for Wide Seafloor Survey –Sea Experiment with two AUVs–," in Proc. MTS/IEEE OCEANS Conf., Apr. 2014, DOI: 10.1109/OCEANS-TAIPEI.2014.6964386.

[25] T. Maki, T. Matsuda, T. Sakamaki, T. Ura, and J. Kojima, "Navigation Method for Underwater Vehicles Based on Mutual Acoustical Positioning With a Single Seafloor Station," IEEE J. Ocean. Eng., vol. 38, no. 1, pp. 167-177, Jan, 2013, DOI: 10.1109/JOE.2012.2210799.

[26] T. Matsuda, T. Maki, T. Sakamaki, and T. Ura, "State Estimation of Multiple Autonomous Underwater Vehicles for Wide Area Survey of Seafloor," MTS/IEEE OCEANS 2013 Bergen, pp.1-9, Jun. 2013, DOI: 10.1109/OCEANS-Bergen.2013.6608192.

[27] T. Matsuda, T. Maki, T. Sakamaki, and T. Ura, "State Estimation and Compression Method for the Navigation of Multiple Autonomous Underwater Vehicles with Limited Communication Traffic," IEEE J. Ocean. Eng., vol. 40, no. 2, pp. 337-348, Apr., 2015, DOI: 10.1109/JOE.2014.2323492.

[28] H. Kondo, T. Ura, and Y. Nose, "Development of an Autonomous Underwater vehicle "Tri-Dog" Toward Practical Use in Shallow Water," Journal of Robotics and Mechatronics, vol.13, no.2, pp.205–211, 2001.

[29] T. Maki, Y. Sato, T. Matsuda, A. Kume, T. Sakamaki, and T. Ura, "AUV Tri-TON -A hover-capable platform for 3D visualization of complicated surfaces," in Proc. Underwater Technology Symposium (UT), March 2013, DOI: 10.1109/UT.2013.6519873.